Constraints in Nonlinear $\mathcal{L}_2$-Stable Networked Control ⋆

Torbjörn Wigren [a]

[a] *Uppsala University, SE-75105, Uppsala, SWEDEN*

Abstract

The paper derives a robust networked controller design method for systems with saturation where the delay is large and unknown, as in unidirectional flow-control. A classical linear robust criterion is first formulated in terms of the sensitivity- and complementary sensitivity functions. Based on the Popov-criterion a new asymptotic constraint is derived, which specifies the minimum amount of low frequency gain in the sensitivity function, to guarantee non-linear closed loop $\mathcal{L}_2$-stability. This result guides the selection of the design criterion, thereby adjusting the linear controller design for better handling of delay and saturation. The controller design method then uses gridding to pre-compute the $\mathcal{L}_2$ stability region. Based on the pre-computed stability region, a robust $\mathcal{L}_2$-stable controller can be selected. Alternatively, an adaptive controller could recompute $\mathcal{L}_2$-stable controllers on-line using the pre-computed stability region. Simulations show that the controller meets the specified stability and performance requirements.

Key words: Delay; Feedback control; Flow control; H_∞-control; $\mathcal{L}_2$-stability; Networked Control; Nonlinear Control; Popov criterion; Robust Control; Saturation; Sensitivity function.

1 Introduction

The report derives a new low frequency constraint on the sensitivity function valid in case of linear control subject to saturation and a long uncertain delay. This guides the selection of a robust frequency domain H_∞ criterion, to be consistent with the combined effect of saturation and delay. The $\mathcal{L}_2$ stability region of the non-linear closed-loop system is then pre-computed with an algorithm based on the Popov criterion. An $\mathcal{L}_2$ stable and robust feedback controller can then be selected from the pre-computed stability region, either fixed or adaptively. The problem arises e.g. in networked control [8], in flow control [13] and in servo design that involves delay [30].

Networked control addresses control over communication channels, with limited information. In networked control much work has been devoted to finding the minimal information needed for stabilization, see e.g. [2], [9], [18] and [24]. Furthermore, the interplay between the encoding of control information and the controller design provides insights useful for design, see [4] and [12] for some examples. Delay is another important dynamic effect that is present in many networked control systems that are distributed between different nodes. Delay also limits information, since delayed measurements in general become less useful for feedback when the delay increases [5]. Delay problems are e.g. commonplace in the cellular communication field [16], [19], [25]. One particular such case is the internet data flow control problem discussed in [31]. There a saturation appears in the loop since the data flow is one-directional. This is also the case in other types of data flow control problems like in traffic flow control, [14], fluid flow control [29] and in water flow control in hydro-power plants [26]. Saturation is also present in many servo controllers, since the actuator hardware performance always needs to be fully exploited [30].

The first technical contribution of the report derives a low frequency limitation on the loop gain, when the plant delay tends to infinity and the control loop is affected by saturation. The limitation is expressed in terms of the

⋆ This paper was not presented at any IFAC meeting. Corresponding author T. Wigren. Tel. +46-18-4716226. Fax +46-18-511925.

Email address: torbjorn.wigren@it.uu.se (Torbjörn Wigren).

poles and zeros of the loop gain and the maximum slope of the saturating nonlinearity. The result states that in case the static loop gain becomes too large, the Popov criterion [20], [23], [32] does not imply $\mathcal{L}_2$ stability. Put otherwise the low frequency gain cannot become arbitrarily high, a fact that e.g. prevents integrating control. The second technical contribution builds on the first to obtain a corresponding low frequency limitation on the sensitivity function [6], [33]. In case the low frequency gain of the sensitivity function becomes less than a value determined by the maximum slope of the nonlinearity, then the Popov criterion does not imply $\mathcal{L}_2$ stability. The third contribution uses the sensitivity function constraint to design modified frequency domain penalty functions for the applied H_∞ loop shaping controller, thereby adapting the linear design criterion towards the situation with a long unknown delay and saturation. The fourth contribution shows how the $\mathcal{L}_2$ stability region can be pre-computed. The combination of the technical contributions then result in a novel controller design procedure for the problem at hand, by selection of a controller from the pre-computed stability region. The proposed method accounts for nominal delays by means of a rational delay approximation [28].

The general literature on linear control with saturation, and linear control with delay is vast, see e.g. [3], [5], [17], [30]. However, the combined effect of long delay and saturation does not seem to have been much addressed, in particular not with frequency domain techniques as in the present report. The advantages of the proposed controller design scheme as compared to the lead-lag controller of [31] include an enhanced robustness. The linear controller is far less complex than alternatives for robust nonlinear control of the plant in the literature, see e.g. [10], [14], [15]. The proposed controller is also designed using frequency domain arguments, a fact that is beneficial when practical engineering problems are encountered. On the downside, the proposed method is not optimal in the $\mathcal{L}_2$ sense, meaning that the full performance potential may not be exploited.

The numerical example of the report treats data flow control over the internet [25]. This is particularly difficult over wireless interfaces due to the rapidly varying radio conditions. Then the adaptive queue management (AQM) algorithms can benefit from fallback servo control of the priority queues in the base stations, as in [31]. The numerical evaluation builds on the servo control model of that paper.

The organisation of the report is as follows. Section 2 defines the controller design problem. The linear part of the joint plant model is derived in section 3. Chapter 4 introduces $\mathcal{L}_2$ stability while sections 5 and 6 derive the main results and formulate the controller design procedure. Section 7 presents the numerical evaluation for the networked data flow control problem. Conclusions end the report in section 8.

2 The robust networked control problem

2.1 The networked system

The nonlinear networked system treated in the report is depicted in Fig. 1 and Fig. 2. As can be seen the input $u(t)$ is subject to a static nonlinear saturation and a delay T_p. It is assumed that the delay is uncertain. The output is also affected by a disturbance w. This disturbance is used to formulate the feedback control objective.

2.2 Controller design outline

The proposed controller design method consists of three main steps.

In the first step a linear single-input-single-output (SISO) control problem is formulated in terms of the penalty signals z_1, z_2 and z_3 that are augmented to the plant as illustrated in Fig. 1 , see e.g. [6] or [7] for details. The nonlinearity is not accounted for yet. The applied H_∞ controller design method is based on state space techniques, therefore the quantities of Fig. 1 are used to construct a corresponding joint linear state space model.

In the second step the non-linear closed loop system of Fig. 1 is considered, where a static nonlinear saturation is present in the feedback path. The controller design is based on a new constraint derived in the report, that specifies the minimum amount of low-frequency gain allowed in the sensitivity function to enable closed loop $\mathcal{L}_2$ stability.

The third step of the controller design applies the input-output stability version of the Popov criterion of [30] to pre-compute the exact $\mathcal{L}_2$ stability region. Controller parameters are then selected in that region, either fixed or adaptively selected on-line [1], [11].

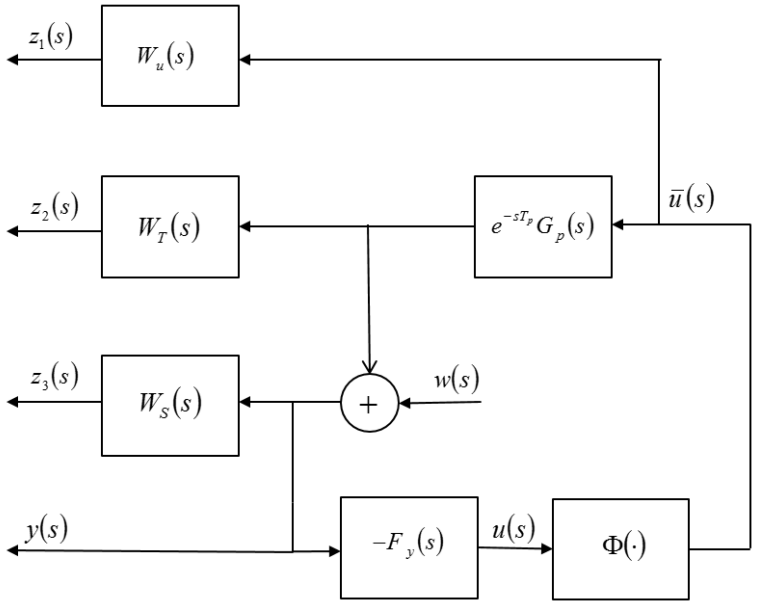

Fig. 1. Block diagram of the system, together with the augmented outputs z_1, z_2 and z_3.

In the report vectors and matrices are marked by boldface characters. Furthermore, the Laplace transform variable s, the differentiation operator p, and the complex angular frequency $j\omega$ are all used, for transfer functions, the time domain counterpart and to address frequency responses.

3 Linear H_∞ feedback control

3.1 Requirements

The control requirements are first expressed neglecting the nonlinearity. The requirements are given in terms of penalties on the sensitivity function

$$S(s) = \frac{1}{1 + F_y(s)G(s)}, \tag{1}$$

the complementary sensitivity function

$$T(s) = \frac{F_y(s)G(s)}{1 + F_y(s)G(s)}, \tag{2}$$

and the transfer function from w to $\bar{u}$

$$G_{w\bar{u}}(s) = -F_y(s)S(s). \tag{3}$$

Here the feedback transfer function $F_y(s)$ is to be determined by the controller design, while the plant transfer function is

$$G(s) = e^{-sT_p}G_p(s). \tag{4}$$

T_p denotes the delay of the plant, where the subscript $_p$ indicates the plant. The control objective variables z_1, z_2 and z_3 defined by Fig. 1 are used to formulate the H_∞ optimization problem that leads to the controller. The H_∞

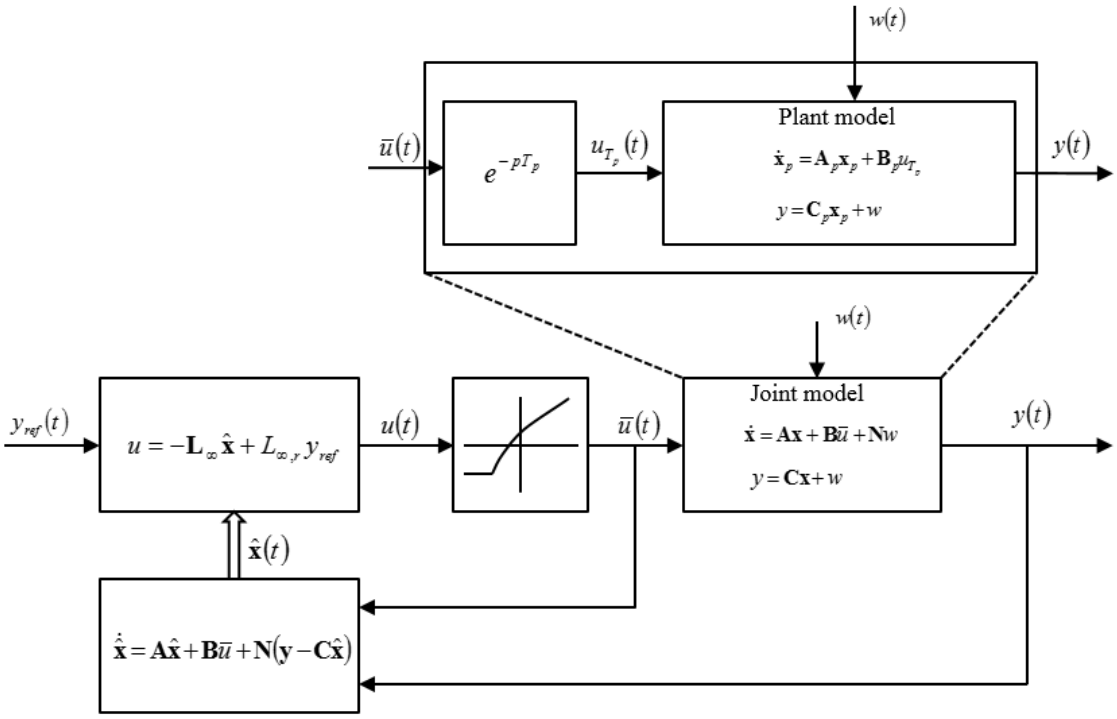

Fig. 2. Block diagram of the H_∞ feedback control problem. The parts broken out, indicated with dashed lines, show the details of the plant model. The plant model variables are marked with the subscript $_p$, while the joint model does not have a subscript. The joint model also contains the dynamics that generate the control objective signals z_1, z_2 and z_3.

requirements on the closed loop system now follow as [7].

$$\begin{aligned} |W_S(j\omega)S(j\omega)| &< \gamma \\ |W_T(j\omega)T(j\omega)| &< \gamma \\ |W_{\bar{u}}(j\omega)G_{w\bar{u}}(j\omega)| &< \gamma. \end{aligned} \tag{5}$$

The selection of the penalty functions $W_S(j\omega)$, $W_T(j\omega)$ and $W_{\bar{u}}(j\omega)$ are further discussed in section 5, where new additional constraints on their selection are derived. The quantity γ is a design parameter, also further discussed below. When the loop of Fig. 1 is closed, neglecting the nonlinearity, it follows that

$$\mathbf{z}(s) = \begin{pmatrix} z_1(s) \\ z_2(s) \\ z_3(s) \end{pmatrix} = \begin{pmatrix} W_{\bar{u}}(s)G_{w\bar{u}}(s) \\ -W_T(s)T(s) \\ W_S(s)S(s) \end{pmatrix} w(s)$$

$$= \mathbf{G}_{ec}(s)w(s), \tag{6}$$

where the transfer function $\mathbf{G}_{ec}(s)$ can be directly used to quantify criteria on the control objective variables z_1, z_2 and z_3.

3.2 Linear state space model components

A block diagram of the state space model of the closed loop system appears in Fig. 2. The joint linear plant dynamics is defined by the matrices $\mathbf{A}$, $\mathbf{B}$, and $\mathbf{N}$, while the plant dynamics excluding the delay is given by $\mathbf{A}_p$, $\mathbf{B}_p$ and $\mathbf{N}_p$. The plant dynamics is excited by the scalar control signal u_{T_p}. The scalar output vector y is a linear function of the state vector $\mathbf{x}_p$, the disturbance vector w, $\mathbf{C}_p$, or equivalently of $\mathbf{x}$, w and $\mathbf{C}$. As shown in Fig. 1 the control signal

$\bar{u}$ is subject to the delay block e^{-pT_p} to produce u_{T_p}, where p is the differentiation operator with respect to time t. The control signal u is affected by a saturating static nonlinear function $\Phi(\cdot)$. The controller computes the control signal u from the estimated state vector $\hat{\mathbf{x}}$ and the controller gains $\mathbf{L}_\infty$ and $L_{\infty,r}$ that are computed later in the report. The state observer performs the estimation based on the joint state space model, $\bar{u}$ and y. The reason why $\mathbf{N}$ can be directly used for state observation is that the feedback controller design problem below is formulated on innovations form [7]. The static nonlinearity is known, hence the controller can generate $\bar{u}$.

The plant model, without delay, is first written in the following state space form.

$$\dot{\mathbf{x}}_p(t) = \mathbf{A}_p\mathbf{x}_p(t) + \mathbf{B}_p u_{T_p}(t). \tag{7}$$

Here $\mathbf{x}_p$ denotes the state of $G_p(s)$ controllable by u_{T_p}. The matrix $\mathbf{A}_p$ describes the dynamic modes of the plant, while the control signal gain vector is given by $\mathbf{B}_p$. The output of the plant is

$$y(t) = \mathbf{C}_p\mathbf{x}_p(t) + w(t). \tag{8}$$

Here $\mathbf{C}_p$ and the disturbance w describe how the states $\mathbf{x}_p$ affect the output y.

The H_∞ controller design accounts for a nominal delay by the use of a rational delay approximation. The Padé approximation [28] can e.g. be used. Contrary to the plant dynamics, the use of a rational delay approximation introduces a direct term in the following state space model

$$\begin{aligned} \dot{\mathbf{x}}_{T_p}(t) &= \mathbf{A}_{T_p}\mathbf{x}_{T_p}(t) + \mathbf{B}_{T_p}\bar{u}(t) \\ u_{T_p}(t) &= \mathbf{C}_{T_p}\mathbf{x}_{T_p}(t) + D_{T_p}\bar{u}(t), \end{aligned} \tag{9}$$

Here $\mathbf{x}_{T_p}$ are the states needed to describe the delay, $\bar{u}$ is the corresponding input, while the approximated delay dynamics is parameterized by the system matrices $\mathbf{A}_{T_p}$, $\mathbf{B}_{T_p}$, $\mathbf{C}_{T_p}$, and D_{T_p}. See Fig. 2 for details.

The next step is to write down the state space realizations of the performance variables z_1, z_2 and z_3 of Fig. 1. These models are given by

$$\begin{aligned} \dot{\mathbf{x}}_{W_{\bar{u}}}(t) &= \mathbf{A}_{W_{\bar{u}}}\mathbf{x}_{W_{\bar{u}}}(t) + \mathbf{B}_{W_{\bar{u}}}\bar{u}(t) \\ z_1(t) &= \mathbf{C}_{W_{\bar{u}}}\mathbf{x}_{W_{\bar{u}}}(t) + D_{W_{\bar{u}}}\bar{u}(t), \end{aligned} \tag{10}$$

$$\begin{aligned} \dot{\mathbf{x}}_{W_T}(t) &= \mathbf{A}_{W_T}\mathbf{x}_{W_T}(t) + \mathbf{B}_{W_T}\mathbf{C}_p\mathbf{x}_p(t) \\ z_2(t) &= \mathbf{C}_{W_T}\mathbf{x}_{W_T}(t) + D_{W_T}\mathbf{C}_p\mathbf{x}_p(t), \end{aligned} \tag{11}$$

$$\begin{aligned} \dot{\mathbf{x}}_{W_S}(t) = &\quad \mathbf{A}_{W_S}\mathbf{x}_{W_S}(t) + \mathbf{B}_{W_S}\mathbf{C}_p\mathbf{x}_p \\ &+\mathbf{B}_{W_S}w(t) \\ z_3(t) &= \mathbf{C}_{W_S}\mathbf{x}_{W_S}(t). \end{aligned} \tag{12}$$

See Fig. 1 for a detailed explanation of (12). Again, $\mathbf{x}_{W_{\bar{u}}}$, $\mathbf{x}_{W_T}$ and $\mathbf{x}_{W_S}$ represent the states of the performance variable dynamics, $\bar{u}$, $\mathbf{x}_p$ and $\mathbf{x}_p$ represent the corresponding inputs, partly expressed in terms of the state $\mathbf{x}_p$ of (8), while the dynamics is parameterized by $\mathbf{A}_{W_{\bar{u}}}$, $\mathbf{B}_{W_{\bar{u}}}$, $\mathbf{C}_{W_{\bar{u}}}$, $D_{W_{\bar{u}}}$, $\mathbf{A}_{W_T}$, $\mathbf{B}_{W_T}\mathbf{C}_p$, $\mathbf{C}_{W_T}$, D_{W_T}, $\mathbf{A}_{W_S}$, $\mathbf{B}_{W_S}\mathbf{C}_p$, and $\mathbf{C}_{W_S}$. See Fig. 2 for details.

3.3 Joint linear state space model

A joint model for the plant is first defined, in order to make the notation more compact. Combining (7) and (9) gives the following joint model, including the delay.

$$\dot{\mathbf{x}}_{FB}(t)$$

$$= \begin{pmatrix} \dot{\mathbf{x}}_p(t) \\ \dot{\mathbf{x}}_{T_p}(t) \end{pmatrix} = \begin{pmatrix} \mathbf{A}_p & \mathbf{B}_p\mathbf{C}_{T_p} \\ \mathbf{0} & \mathbf{A}_{T_p} \end{pmatrix} \begin{pmatrix} \mathbf{x}_p(t) \\ \mathbf{x}_{T_p}(t) \end{pmatrix}$$

$$+ \begin{pmatrix} \mathbf{B}_p D_{T_p} \\ \mathbf{B}_{T_p} \end{pmatrix} \bar{u}(t) = \mathbf{A}_{FB}\mathbf{x}_{FB}(t) + \mathbf{B}_{FB}\bar{u}(t). \tag{13}$$

$$y(t) = \begin{pmatrix} \mathbf{C}_p & \mathbf{0} \end{pmatrix} \begin{pmatrix} \mathbf{x}_p(t) \\ \mathbf{x}_{T_p}(t) \end{pmatrix} + w(t)$$

$$= \mathbf{C}_{FB}\mathbf{x}_{FB} + w(t) \tag{14}$$

The details of the joint model depicted in Fig. 2 can then be defined as

$$\begin{aligned} \dot{\mathbf{x}}(t) &= \mathbf{A}\mathbf{x}(t) + \mathbf{B}\bar{u}(t) + \mathbf{N}w(t) \\ y(t) &= \mathbf{C}\mathbf{x}(t) + w(t). \end{aligned} \tag{15}$$

This is the model upon which the controller design is based. Since the delay is replaced by a rational approximation embedded in the joint state space model (15), a standard H_∞ controller design method can be applied.

Using (10)-(13) it follows that the state and the system matrices of (15) can be written as

$$\mathbf{x} = \begin{pmatrix} \mathbf{x}_{FB}^T & \mathbf{x}_{W_s}^T & \mathbf{x}_{W_T}^T & \mathbf{x}_{W_{\bar{u}}}^T \end{pmatrix}^T \tag{16}$$

$$\mathbf{A} = \begin{pmatrix} \mathbf{A}_{FB} & \mathbf{0} & \mathbf{0} & \mathbf{0} \\ \mathbf{B}_{W_S}\mathbf{C}_{FB} & \mathbf{A}_{W_S} & \mathbf{0} & \mathbf{0} \\ \mathbf{B}_{W_T}\mathbf{C}_{FB} & \mathbf{0} & \mathbf{A}_{W_T} & \mathbf{0} \\ \mathbf{0} & \mathbf{0} & \mathbf{0} & \mathbf{A}_{W_{\bar{u}}} \end{pmatrix} \tag{17}$$

$$\mathbf{B} = \begin{pmatrix} \mathbf{B}_{FB}^T & \mathbf{0} & \mathbf{0} & \mathbf{B}_{W_{\bar{u}}}^T \end{pmatrix}^T \tag{18}$$

$$\mathbf{N} = \begin{pmatrix} \mathbf{0} & \mathbf{B}_{W_S}^T & \mathbf{0} & \mathbf{0} \end{pmatrix}^T \tag{19}$$

$$\mathbf{C} = \begin{pmatrix} \mathbf{C}_{FB} & \mathbf{0} & \mathbf{0} & \mathbf{0}. \end{pmatrix} \tag{20}$$

Note that there are no direct term in the joint model. This gives a strictly proper joint model, a fact that is used in the forthcoming analysis. Note also that the model is in the innovations form used in [7] to design H_∞-controllers.

3.4 H_∞ control

To define the H_∞ optimization problem, a criterion penalizing the control objective signals $z_1(t)$, $z_2(t)$ and $z_3(t)$ is needed. The control objective signals are therefore added to the joint state space model output of (15). The control objective output equation is given by

$$\mathbf{z}(t) = \mathbf{M}\mathbf{x}(t) + \mathbf{D}\bar{u}(t), \tag{21}$$

where $\mathbf{x}(t)$ is given by (16). It follows from (10)-(12) and (16) that

$$\mathbf{M} = \begin{pmatrix} \mathbf{0} & \mathbf{0} & \mathbf{0} & \mathbf{C}_{W_{\bar{u}}} \\ D_{W_T}\mathbf{C}_{FB} & \mathbf{0} & \mathbf{C}_{W_T} & \mathbf{0} \\ \mathbf{0} & \mathbf{C}_{W_S} & \mathbf{0} & \mathbf{0} \end{pmatrix}, \tag{22}$$

$$\mathbf{D} = \begin{pmatrix} D_{W_{\bar{u}}} \\ 0 \\ 0 \end{pmatrix}. \tag{23}$$

The following condition is then introduced to simplify the criterion minimization.

A1) $D_{W_{\bar{u}}} > 0$.

As outlined in [7], A1 implies that the following change of variables is well defined

$$\tilde{u} = \left(\mathbf{D}^T\mathbf{D}\right)^{\frac{1}{2}} \bar{u} + \left(\mathbf{D}^T\mathbf{D}\right)^{-\frac{1}{2}} \mathbf{D}^T\mathbf{M}\mathbf{x}. \tag{24}$$

When (24) is applied to (15)-(20) and (21)-(23), the following transformed system results

$$\begin{aligned} \dot{\mathbf{x}}(t) &= \tilde{\mathbf{A}}\mathbf{x}(t) + \tilde{\mathbf{B}}\tilde{u}(t) + \tilde{\mathbf{N}}w(t) \\ \mathbf{z}(t) &= \tilde{\mathbf{M}}\mathbf{x}(t) + \tilde{\mathbf{D}}\tilde{u}(t) \\ \mathbf{y}(t) &= \tilde{\mathbf{C}}\mathbf{x}(t) + w(t), \end{aligned} \tag{25}$$

where

$$\tilde{\mathbf{A}} = \mathbf{A} - \mathbf{B}\left(\left(\mathbf{D}^T\mathbf{D}\right)^{-1}\mathbf{D}^T\mathbf{M}\right), \tag{26}$$

$$\tilde{\mathbf{B}} = \mathbf{B}\left(\mathbf{D}^T\mathbf{D}\right)^{-\frac{1}{2}}, \tag{27}$$

$$\tilde{\mathbf{N}} = \mathbf{N}, \tag{28}$$

$$\tilde{\mathbf{C}} = \mathbf{C}, \tag{29}$$

$$\tilde{\mathbf{M}} = \left(\mathbf{I} - \mathbf{D}\left(\mathbf{D}^T\mathbf{D}\right)^{-1}\mathbf{D}^T\right)\mathbf{M}, \tag{30}$$

$$\tilde{\mathbf{D}} = \mathbf{D}\left(\mathbf{D}^T\mathbf{D}\right)^{-\frac{1}{2}}. \tag{31}$$

Note that A1 also implies that

$$\tilde{\mathbf{D}}^T(\,\tilde{\mathbf{M}}\;\tilde{\mathbf{D}}\,) = (\,\mathbf{0}\;\mathbf{I}\,). \tag{32}$$

As a further prerequisite, introduce the condition

A2) $(\mathbf{A}, \mathbf{B})$ is stabilizable, $(\mathbf{A}, \mathbf{M}\mathbf{M}^T)$ is detectable, and $\tilde{\mathbf{A}} - \tilde{\mathbf{N}}\tilde{\mathbf{C}}$ is asymptotically stable.

The H_∞-optimization problem and its solution as used in this report can now be stated:

Lemma 1 ([7], Theorem 10.1): Consider the system (25). Assume that A1 and A2 hold. Let $\hat{\gamma}$ be the minimum value of γ for which $\mathbf{S} = \mathbf{S}^T \geq \mathbf{0}$ satisfy the Riccati-equation

$$\tilde{\mathbf{A}}^T\mathbf{S} + \mathbf{S}\tilde{\mathbf{A}} + \tilde{\mathbf{M}}^T\tilde{\mathbf{M}} + \mathbf{S}\left(\gamma^{-2}\tilde{\mathbf{N}}\tilde{\mathbf{N}}^T - \tilde{\mathbf{B}}\tilde{\mathbf{B}}^T\right)\mathbf{S} = \mathbf{0}.$$

Assume that the states are estimated by

$$\dot{\hat{\mathbf{x}}}(t) = \tilde{\mathbf{A}}\hat{\mathbf{x}}(t) + \tilde{\mathbf{B}}u(t) + \tilde{\mathbf{N}}\left(\mathbf{y}(t) - \tilde{\mathbf{C}}\hat{\mathbf{x}}(t)\right).$$

If $\mathbf{x}(0) = \mathbf{0}$, and if the feedback is selected as

$$\tilde{u}(t) = -\mathbf{L}_\infty\hat{\mathbf{x}}(t) = -\tilde{\mathbf{B}}\mathbf{S}\hat{\mathbf{x}}(t),$$

then this feedback minimizes the H_∞ criterion

$$V_\infty = \|\mathbf{G}_{ec}\|_\infty = \max_\omega \bar{\sigma}\left(\mathbf{G}_{ec}(i\omega)\right).$$

Here $\bar{\sigma}(\cdot)$ denotes the maximum singular value.

In the present report $\tilde{\mathbf{D}}^T\tilde{\mathbf{D}} = 1$ holds. This means that $\mathbf{B} = \tilde{\mathbf{B}}$ and the feedback gain $\mathbf{L}_\infty$ can be directly applied to the original system without any back-transformation using (24).

3.5 The resulting frequency domain closed loop system

In the following sections frequency-domain input-output stability results will be applied to complete the $\mathcal{L}_2$-stable controller design procedure. The transfer function of the feedback controller is therefore needed. To compute it, it is noted that the state space model that defines the controller of Lemma 1 can be written as

$$\begin{aligned} \dot{\hat{\mathbf{x}}}(t) &= \left(\tilde{\mathbf{A}} - \tilde{\mathbf{B}}\tilde{\mathbf{B}}^T\mathbf{S} - \tilde{\mathbf{N}}\tilde{\mathbf{C}}\right)\hat{\mathbf{x}}(t) + \tilde{\mathbf{N}}y(t) \\ u(t) &= -\mathbf{L}_\infty\hat{\mathbf{x}}(t). \end{aligned} \tag{33}$$

The transfer function from $y(t)$ to $u(t)$ then follows as

$$F_y(s) = \mathbf{L}_\infty\left(sI - \tilde{\mathbf{A}} + \tilde{\mathbf{B}}\tilde{\mathbf{B}}^T\mathbf{S} + \tilde{\mathbf{N}}\tilde{\mathbf{C}}\right)^{-1}\tilde{\mathbf{N}} \tag{34}$$

The control signal $u(s)$ is hence computed as

$$u(s) = L_{\infty,r}y_{ref}(s) - F_y(s)y(s). \tag{35}$$

Equation (35) together with Fig. 1, results in the frequency domain block diagram of Fig. 3. The transfer function $G_p(s)$ is known and is represented by the states of (7).

4 $\mathcal{L}_2$ stability conditions

4.1 Static nonlinearity

The static non-linearity of the loop first needs to be defined. The static nonlinear saturation transforms $u(t)$ into $\bar{u}(t) = \Phi(u(t))$, where

$$\Phi(u) = \begin{cases} \bar{u}_{max}, & u \geq u_{max} \\ \varphi(u), & u_{min} < u < u_{max} \\ \bar{u}_{min}, & u \leq u_{min}. \end{cases} \tag{36}$$

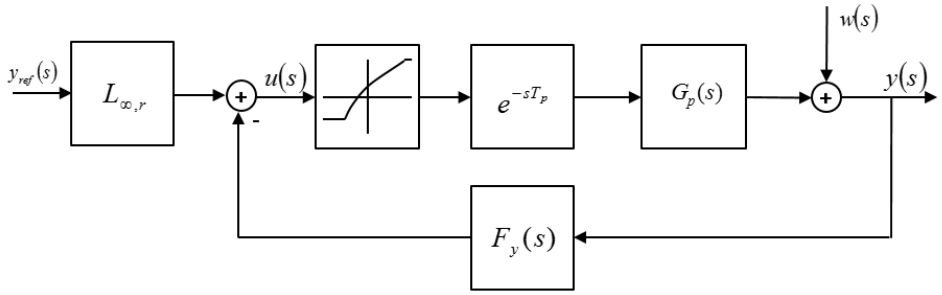

Fig. 3. Block diagram of the networked control system in the frequency domain.

4.2 $\mathcal{L}_p$ definitions

The linear H_∞-controller of Lemma 1 is then applied to the nonlinear system of Fig. 2. To address stability in the presence of delay it is now suitable to apply the input-output stability version of the SISO Popov-criterion given in e.g. [30]. The following definitions are needed to state the result.

Definition 1: For all $p \in [0,\infty)$, $\mathcal{L}_p[0,\infty)$ denotes the set of all measurable functions $f(.) : [0,\infty) \to R$, such that

$$\|f(.)\|_p^p = \int_0^\infty |f(t)|^p dt < \infty.$$

Definition 2: The set of all measurable functions $f(.) : [0,\infty) \to R$, such that their truncations

$$f_T(t) = \begin{cases} f(t), & 0 \le t \le T \\ 0, & t > T \end{cases} \in \mathcal{L}_p[0,\infty),$$

$\forall T$, is denoted the extension $\mathcal{L}_{pe}[0,\infty)$ of $\mathcal{L}_p[0,\infty)$.

Definition 3: The mapping $A : \mathcal{L}_{pe} \to \mathcal{L}_{pe}$ is $\mathcal{L}_p$-stable if i) $Af \in \mathcal{L}_p$ whenever $f \in \mathcal{L}_p$, and ii) there exist finite constants k, c, such that

$$\|Af\|_p \le k\|f\|_p + c, \quad \forall f \in \mathcal{L}_p.$$

Definition 4: $\mathcal{A}$ denotes the set of generalized functions of the form

$$f(t) = \begin{cases} 0, & t < 0 \\ \sum_{i=0}^\infty f_i \delta(t - t_i) + f_a(t), & t \ge 0 \end{cases}$$

where $\delta(.)$ is the unit delta distribution, t_i are non-negative constant delays, $f_a(t)$ is measurable and

$$\sum_{i=0}^\infty |f_i| < \infty, \quad \int_0^\infty |f_a(t)|dt < \infty.$$

Definition 5: $\hat{\mathcal{A}}$ denotes the set of all function $\hat{f} : C_+ \to C$ that are Laplace transforms of elements of $\mathcal{A}$.

4.3 The Popov criterion

The Popov criterion can now be formulated:

Lemma 2 (Popov Criterion, [30] Theorem 6.7.63): Consider the system of Fig. 4. Assume that the inverse Laplace transform of the transfer function $\hat{g}(s)$ fulfils

$$g(\cdot) \in \mathcal{A}, \quad \dot{g}(\cdot) \in \mathcal{A},$$

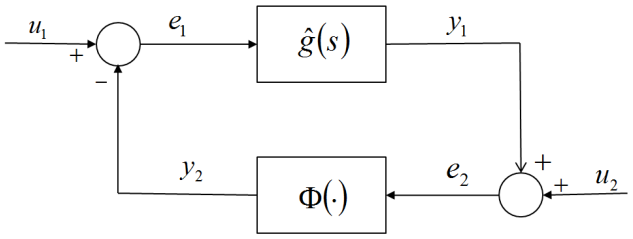

Fig. 4. Block diagram for which the Popov criterion is valid.

that the time invariant static nonlinearity $\Phi(.)$ fulfils

$$0 \leq \sigma\Phi(\sigma) \leq k\sigma^2,$$

and that $\dot{u_2} \in \mathcal{L}_2$. Under these conditions the system is $\mathcal{L}_2$-stable if there exist constants q, δ, such that the Popov plot

$$\omega \in [0, \infty) \rightarrow Re[\hat{g}(j\omega)] + j\omega Im[\hat{g}(j\omega)] \in C$$

is entirely to the right of a line through $-1/k + \delta + j0$ with slope $1/q$, for some $q \geq 0$ and some $\delta > 0$.

Proof: See [30], section 6.7.

Note that the geometrical condition on the Popov plot is equivalent to the following inequality

$$Re[(1 + j\omega q)\hat{g}(j\omega)] + \frac{1}{k} \geq \delta > 0, \ \forall\omega \geq 0, \ q > 0. \tag{37}$$

5 Low frequency sensitivity function constraints

This section derives the main results of the report and sets the stage for the second step of the proposed controller design procedure. A first Theorem shows that the Popov criterion is valid for the networked control system. A second Theorem states how much low frequency loop gain that can be present without invalidating the Popov-criterion of Theorem 1, in the limiting case when $T_p \rightarrow \infty$. This result then leads to a third Theorem that provides new constraints on the sensitivity function. The sensitivity function constraints in turn lead to new selection principles for $W_S(s)$ and $W_T(s)$ of (5). This serves to adapt the linear H_∞ controller design to better fit the nonlinear system of Fig. 2 - Fig. 4.

5.1 Conditions on the control system

This subsection introduces the conditions needed to apply Lemma 2 to the control system of Fig. 2. The analysis does not allow a time varying system, hence the following condition is needed.

A3) The delay T_p is constant.

Since the sector condition of (36) reads

$$0 \leq \sigma\Phi(\sigma) \leq 1\sigma^2, \tag{38}$$

it follows from Lemma 2 that the loop gain $\hat{g}(s)$ needs to be strictly proper and have all poles strictly in the left half plane. Fig. 3, Fig. 4, and (4) show that the loop gain $\hat{g}(s)$ is given by

$$\hat{g}(s) = G(s)F_y(s) = e^{-sT_p}G_p(s)F_y(s). \tag{39}$$

Noting again that (33) has no direct term, $F_y(s)$ s strictly proper by construction. The following conditions are therefore needed to ensure that $g(\cdot) \in \mathcal{A}$ and $\dot{g}(\cdot) \in \mathcal{A}$

A4) $G_p(s)$ is proper with all poles of $G_p(s)$ and $G_p^{-1}(s)$ strictly in the left half plane.
A5) $F_y(s)$ has all poles strictly in the left half plane.

In addition to A3, A4 and A5, the following disturbance signal conditions are needed, considering the fact that $\dot{u_2} \in \mathcal{L}_2$ is a requirement of Lemma 2.

A6) $y_{ref} \in \mathcal{L}_2$ and $\dot{y}_{ref} \in \mathcal{L}_2$.
A7) $w/G_p \in \mathcal{L}_2$.

The conditions A3-A7 are straightforward to explain and check. The stability requirements of A4 and A5 can be checked before and during the controller design. The condition A6 and A7 are needed to ensure that u_1, u_2 and $\dot{u}_2$ expressed in terms of y_{ref} and w all have proper Laplace transforms. Put otherwise A6 and A7 require a sufficiently large roll-off of the high frequency contents. The reason why A7 needs to involve filtering is due to the loop transformations performed in the proof below. A7 is also the reason why the plant transfer function $G_p(s)$ needs to be minimum phase.

5.2 Closed loop $\mathcal{L}_2$ stability

The following result now holds:

Theorem 1: Consider the control system of Fig. 2 and assume that the conditions A3)-A7) hold. Then the control system is $\mathcal{L}_2$-stable if there exist constants q, $\delta > 0$, such that the Popov plot of

$$\hat{g}(s) = e^{-sT_p} G_p(s) F_y(s),$$

given by

$$\omega \in [0, \infty) \rightarrow Re[\hat{g}(j\omega)] + j\omega Im[\hat{g}(j\omega)] \in C$$

is entirely to the right of a line through $-1 + \delta + j0$ with slope $1/q$, for some $q \geq 0$ and some $\delta > 0$.

Proof: See appendix A.

5.3 Low frequency loop gain limitation

The interest here is to derive low frequency *limitations* on $\hat{g}(s)$, therefore it is desirable to study situations where Theorem 1 *does not hold*. The value of the Popov curve is therefore addressed on the negative real axis of the complex plane. This choice is geometrically obvious since the Popov limitation line is allowed to rotate around the point $-1/k + \delta + j0$. First, the following condition is needed to ensure that there is at least one intersection with the negative real axis

A8) The Popov-plot intersects the negative real axis at least once.

The condition for the Popov plot of Theorem 1 to intersect the negative real axis is

$$\arg\left(Re[\hat{g}(j\omega)] + j\omega Im[\hat{g}(j\omega)]\right) = -\pi. \tag{40}$$

Since $\omega = 0$ represents the static gain, this solution can be excluded and it follows that (40) is equivalent to

$$Re[\hat{g}(j\omega)] < 0, \quad Im[\hat{g}(j\omega)] = 0. \tag{41}$$

Defining

$$\hat{g}(s) = e^{-sT_p} \hat{g}_o(s) \tag{42}$$

implies that

$$|\hat{g}_o(j\omega)| \sin\left(\arg(\hat{g}_o(j\omega) - \omega T_p)\right) = 0, \tag{43}$$

$$|\hat{g}_o(j\omega)|\cos\left(\arg(\hat{g}_o(j\omega)-\omega T_p)\right)<0. \tag{44}$$

The blocks $G_p(s)$ and $F_y(s)$ of $\hat{g}_o(s)$ are then parameterized in terms of their poles, zeros and a gain parameter

$$G_p(s)=G_{p,o}\frac{(s+b_1)...(s+b_{nb})}{(s+a_1)...(s+a_{na})} \tag{45}$$

$$F_y(s)=F_{y,o}\frac{(s+d_1)...(s+d_{nd})}{(s+c_1)...(s+c_{nc})}. \tag{46}$$

The conditions A9 and A10 are also introduced

A9) Complex poles and zeros of $G_p(s)$ appear in complex conjugate pairs and $G_{p,o}>0$.
A10) Complex poles and zeros of $F_y(s)$ appear in complex conjugate pairs, $|Re[d_i]|>0$, $i=1,...,nd$, $F_{y,o}>0$, and the number of non-minimum phase zeros of $F_y(s)$ is even.

The following result can now be proved:

Theorem 2: Consider the system given by Fig. 2, (45) and (46). Assume that the conditions A3-A10 hold and that $T_p\to\infty$. Then the Popov criterion of Theorem 1 cannot imply $\mathcal{L}_2$-stability in case

$$\lim_{\omega\to 0} Re[G_p(j\omega)F_y(j\omega)]=G_p(0)F_y(0)$$

$$=G_{p,o}F_{y,o}\frac{b_1...b_{nb}d_1...d_{nd}}{a_1...a_{na}c_1...c_{nc}}\geq\frac{1}{k}.$$

Proof: See appendix B.

It follows from the derivation, A9 and A10 that the result hold also for pairs of complex conjugate zeros and poles. It is also stressed that the appearance of the static loop gain in Theorem 2 is a consequence of the proof. It would not have been possible to start with the static case, since that part of the Popov curve is located at the positive real axis. Note that the non-minimum phase requirement of A10 ensures the positivity of the low frequency loop gain limitation of Theorem 2.

Theorem 2 states when the Popov criterion is invalidated, possibly destroying stability of the closed loop system. In particular, it can be seen that Theorem 2 prevents the poles of the system and the feedback controller to be arbitrarily close to the imaginary axis. On the negative real axis this represents a direct limitation of the low frequency loop gain. The result is more restrictive than the Popov criterion itself since poles arbitrarily close to the imaginary axis is not allowed.

Although the Popov criterion is not necessary for stability, Theorem 2 indicates that integrating control may be troublesome in combination with saturation and long delays. Although based purely on numerical results, this fact actually governed the design of [31]. More research is however needed to formally clarify the sufficiency and necessity of Theorem 2, with respect to $\mathcal{L}_2$ stability.

The next question is how the insight provided by Theorem 2 can be used to tune the controller proposed in the report. This is the topic of the next subsection.

5.4 The low frequency sensitivity function constraint

The performance of the controller proposed in the report is tied to the selection of $W_S(j\omega)$, $W_T(j\omega)$ and $W_{\bar{u}}(j\omega)$ of (5). Since the low frequency gain can be specified by the selection of the sensitivity function the implications of Theorem 2 on $S(s)$ is addressed. It holds that

$$S(s)=\frac{1}{1+e^{-sT_p}F_y(s)G_p(s)}=\frac{1}{1+\hat{g}(s)}. \tag{47}$$

To see the implications of Theorem 2, (47) is solved for $\hat{g}(s)$ and the limit when $\omega \to 0$ of Theorem 2 is used to obtain

$$\frac{1}{S(0)} - 1 = \hat{g}(0) = G_p(0)F_y(0)$$

$$= G_{p,o}F_{y,o}\frac{b_1...b_{nb}d_1...d_{nd}}{a_1...a_{na}c_1...c_{nc}} \geq \frac{1}{k}. \tag{48}$$

Solving for $S(0)$ proves

Theorem 3: Consider the system given by Fig. 2, (45) and (46). Assume that the conditions A3-A10 hold and that $T_p \to \infty$. Then the Popov criterion of Theorem 1 cannot imply $\mathcal{L}_2$-stability in case

$$S(0) = \frac{a_1...a_{na}c_1...c_{nc}}{a_1...a_{na}c_1...c_{nc} + G_{p,o}F_{y,o}b_1...b_{nb}d_1...d_{nd}}$$

$$\leq \frac{k}{k+1}.$$

The low frequency gain of the sensitivity function is hence limited from below by the maximum slope of the non-linearity. The limiting value for $k = 1$ is -6 dB. Only in case $k \to 0$ is integral control allowed. It can also be noted that when $T_p \to \infty$ or $k \to 0$ the system tends to open loop operation.

It needs to be understood that Theorem 3 provides an asymptotic result for very large delays. The asymptotic region is often approached relatively slowly, meaning that for moderate delays and uncertainties the design can be significantly less restrictive than indicated by Theorem 3. In practice the important thing to keep in mind is to avoid a too small low frequency gain of the sensitivity function. Ways to achieve this will be addressed next.

5.5 Penalty function selection

It is clear that in order to circumvent Theorem 3 and to enable the Popov criterion of Theorem 1 to be applied to prove $\mathcal{L}_2$ stability, $S(0)$ needs to be prevented from becoming too small. By (5) it then follows that $W_S^{-1}(j\omega)$ must remain strictly greater than 0 when $\omega \to 0$. Hence the sensitivity function penalty needs to fulfil

$$W_S^{-1}(0) > w_{S,o}^{-1} > 0, \tag{49}$$

where $w_{S,o}$ is a positive scalar selected by the designer. For higher frequencies, $S(s)$ can be designed according to standard procedures, see e.g. [6], [7]. The requirement provided by $W_T(s)$ of (5) on $T(s)$ needs to be consistent with (49) since $S(s) + T(s) = 1$.

6 Pre-computed $\mathcal{L}_2$-stable controller design

Now, in case a $W_S(s)$ is selected such that the limitation of Theorem 3 can be circumvented when computing the controller using Lemma 1, $\mathcal{L}_2$-stability should be attainable using Theorem 1. Note that such a proof is very important also in engineering applications since a system that is not globally stable cannot be guaranteed to operate according to the specifications at all times. Theorem 3 therefore provides a way to avoid one potentially very serious engineering obstacle when the delay is large and a saturation affects the feedback loop. The question that remains to be solved is then how to select the design variables so that a feedback is obtained that fulfils Theorem 1, robustly for a range of delays around the nominal one.

6.1 Pre-computation of the $\mathcal{L}_2$ stability region

The idea is to pre-compute the $\mathcal{L}_2$ stability region, as a function of a selected set of design variables and system parameters. The stability region is here defined by the maximal allowed feedback delay of the actual system, $\theta_{\mathcal{L}_2} = T_p$, that renders $\mathcal{L}_2$ stability. The use of other variables than T_p to quantify the stability region is of course also possible. The set of design variables and system parameters is denoted by θ_d. The algorithm (50) computes $\max \theta_{\mathcal{L}_2}(\theta_d)$, such that the closed loop non-linear feedback system is $\mathcal{L}_2$ stable for all $0 < \theta_{\mathcal{L}_2} < \max \theta_{\mathcal{L}_2}(\theta_d)$. The algorithm is a straightforward application of Theorem 1 and (37). It is defined as a search over the grid of design variables and system parameters, $\theta_{d,grid_d}$, the grid of the uncertainty, $\theta_{\mathcal{L}_2,grid_{\mathcal{L}_2}}$, a grid of the slope of the Popov line, q_{grid_q}, and a grid over the angular frequency, ω_{grid_ω}. The pseudo-code of the algorithm is

for $grid_d = 1, \cdots, grid_{d,max}$

  $\theta_{\mathcal{L}_2,found} = false$

  $grid_{\mathcal{L}_2} = 0$

  while $\theta_{\mathcal{L}_2,found} = false$ and $grid_{\mathcal{L}_2} < grid_{\mathcal{L}_2,max}$

    $grid_{\mathcal{L}_2} = grid_{\mathcal{L}_2} + 1$

    $q_{found} = false$

    $grid_q = 0$

    while $q_{found} = false$ and $grid_q < grid_{q,max}$

      $grid_q = grid_q + 1$

      if $Re[(1 + j\omega q_{grid_q})\hat{g}(j\omega_{grid_\omega}, \theta_{d,grid_d}, \theta_{\mathcal{L}_2,grid_{\mathcal{L}_2}})]$

        $+1/k > 0, \quad \forall\ \omega_{grid_\omega} \geq 0$

        $q_{found} = true$

      end

    end

    if $q_{found} = false$

      $\max \theta_{\mathcal{L}_2,grid_{\mathcal{L}_2}}(\theta_{d,grid_d}) = \theta_{\mathcal{L}_2,grid_{\mathcal{L}_2}}$

      $\theta_{\mathcal{L}_2,found} = true$

    end

  end

end. (50)

The subscript $_{found}$ denotes a boolean variable, while $_{max}$ denotes the upper limit of each grid. For each grid point of θ_d, the algorithm scans $\theta_{\mathcal{L}_2}$ upwards on the uncertainty grid. For each such point, q of Theorem 1 is scanned upwards on its grid. For each value of q, (37) is checked for all ω on its grid. If a q is found such that (37) is met, Theorem 1 holds for the specific value of the uncertainty and the scan proceeds. If no q is found such that (37) holds, the scan for the particular specification parameter grid point is completed and the maximum uncertainty is determined. A similar scheme is used in [31].

6.2 Controller design procedure

The controller design procedure can now be summarized.

First penalty functions $W_S(j\omega)$, $W_T(j\omega)$ and $G_{w\bar{u}}(j\omega)$ are selected that express the control objectives and that also ensure that (49) is fulfilled. This is done with guidance from Theorem 3, using prior information of the plant. This defines the joint plant model that is used for H_∞ controller design.

Secondly, the set of design variables of the pre-computation is selected and (50) is run. For each set of parameters on the total grid an H_∞ problem is solved and the Popov inequality (37) is checked. The $\mathcal{L}_2$ stability $\max \theta_{\mathcal{L}_2}(\theta_d)$ is stored for each grid point.

Thirdly, an $\mathcal{L}_2$ stable controller can then be selected or computed on-line in an adaptive scheme [1], [11]

7 Numerical results from wireless data flow control

7.1 The plant

Cellular mobile broadband relies on internet flow control to ensure that there is enough data available in the base station to send over the wireless downlink interface at any point in time. For this reason the base station is equipped with buffers, often denoted priority queues. These buffers compensate for the rapid variations of the wireless radio connection that is caused by fading. The level of data in each buffer needs to be controlled tightly, to as low a level as possibly to minimize delay at the same time as empty buffers are avoided when there is data to transmit in the upstream node closer to the data source. The requirements on flow control will become more stringent in the 5G cellular systems that are now in development since the round trip delay requirements are expected to become much more stringent [22]. The reason for this is to open up for new applications, for example haptic control enabling remote surgery, advanced gaming, and automotive collision avoidance [21].

Wireless internet flow control exploit so called adaptive queue management (AQM) [25]. AQM operates by intentional discard of internet packets in the priority queues when there is a need to reduce the incoming data rates to the priority queues. Recently, it was found that conventional AQM is sometimes unable to meet latency requirements when internet applications simultaneously start many parallel flows [31]. A networked data flow controller for support of an underlying adaptive queue management (AQM) controller was therefore developed in [31]. This section builds on the plant model of [31] for illustration of the controller design method proposed in this report.

The controller is located in a node before the base station node. The base station node contains the priority queues and the wireless interface. The downlink transport network transports the internet packets to the queues with a rate equal to the control signal of the controller. Since the data volume of the queue is the integral of the difference between the control signal bit rate and the emptying bit rate, the low frequency gain conditions of Theorem 3 may appear to be violated in open loop. However, due to the packet drops introduced by the underlying AQM controller, there is already a leakage in the integration. A linear model of a queue controlled by AQM is then,

$$\frac{dy(t)}{dt} = u(t - T_p) - b(t) + \hat{b}(t) - \varepsilon y(t) + w(t). \tag{51}$$

Here $y(t)$ is the data volume of the controlled queue in the base station node, $u(t - T_p)$ is the delayed control signal (bit rate) from the transmitting node that sends data over the transport network to the base station, T_p is the sum of packet delay in the downlink transport network (T_{dl}) and queue level measurements being sent back to the controller over the uplink transport network (T_{ul}), $b(t)$ is the wireless bit rate emptying the queue, ε is the proportional packet drop-rate and $w(t)$ is an additive disturbance that models several significant imperfection of (52), discussed in section 7.2 below. The quantity $\hat{b}$ represents the effect of feed forward control for compensation of $b(t)$ as in [31], see [26] and [27] for more general techniques for that problem. Since the data flow is one directional there is also a saturation in the loop, located in the downlink transport network. The feedback plant model of Fig. 2 is therefore applicable with

$$G_p(s) = \frac{1}{s + \varepsilon} e^{-sT_p}, \tag{52}$$

$$T_p = T_{dl} + T_{ul}, \tag{53}$$

$$\Phi(u) = \begin{cases} \bar{u}_{max}, & u \geq u_{max} \\ u, & 0 < u < u_{max} \\ 0, & u \leq 0. \end{cases} \tag{54}$$

This means that $k = 1$. u_{max} is large and does not affect the system in this example.

In order to compute the controller for a selected designing delay T_p^d, the following rational fourth order Pade approximation is used to model the delay dynamics

$$G_{T_p}(s) =$$

$$\frac{(T_p^d)^4 s^4 - 20(T_p^d)^3 s^3 + 180(T_p^d)^2 s^2 - 840 T_p^d s + 1680}{(T_p^d)^4 s^4 + 20(T_p^d)^3 s^3 + 180(T_p^d)^2 s^2 + 840 T_p^d s + 1680}. \tag{55}$$

The designing delay is in general not equal to the true delay T_p of the plant.

7.2 Controller design

The plant, i.e. the controlled priority queue, is affected by several disturbances. The paper [31] compensated for the wireless bit rate emptying the queue by means of feed forward control. Feed forward control is not within the scope of this report. Instead, the focus is on imperfections and disturbances affecting the plant model (52) directly. Therefore, it is assumed that the feed forward is close to perfect so that $b(t) \approx \hat{b}(t)$, with imperfections of the feed forward being absorbed in $w(t)$. The other disturbances modeled by $w(t)$ include the far from perfect linearity assumption expressed by the constant ε. In practice ε may e.g. vary over time. What is sometimes more important is the fact that occasional large AQM discards may occur, due to significant overload and other reasons.

To perform the controller design, the transfer functions for $W_S(s)$, $W_T(s)$ and $W_{\bar{u}}(s)$ need to be specified. The key here is to select $W_S(s)$ in line with Theorem 3 and (49). To do so the following penalty can be used

$$W_S(s) = \frac{W_S(0)(\omega_{S,den}^2/\omega_{S,num})(s + \omega_{S,num})}{s^2 + 2\xi_{S,den}\omega_{S,den} + \omega_{S,den}^2}. \tag{56}$$

Here $\omega_{S,num}$ and $\omega_{S,den}$ are angular frequency breakpoints, while $\xi_{S,den}$ denotes the damping of the filter. The restriction $\omega_{S,den} < \omega_{S,num}$ is used, which means that $W_S^{-1}(s)$ starts at the static gain $1/W_S(0)$, then breaks upwards at $\omega_{S,den}$ after which the increase is reduced at $\omega_{S,num}$. The requirement of Theorem 3 can hence be fulfilled. $W_T(s)$ is selected in the usual way to ensure robustness against high frequency dynamics,

$$W_T(s) = \frac{W_T(0)(s^2 + 2\xi_{T,num}\omega_{T,num}s + \omega_{T,num}^2)}{s^2 + 2\xi_{T,den}\omega_{T,den} + \omega_{T,den}^2}. \tag{57}$$

Here $\omega_{T,num}$ and $\omega_{T,den}$ are angular frequency breakpoints, while $\xi_{T,num}$ and $\xi_{T,den}$ denote the damping of the filters. In this case the restriction $\omega_{T,num} < \omega_{T,den}$ is used, which means that $W_T^{-1}(s)$ starts at the static gain $1/W_T(0)$, then breaks down at $\omega_{T,num}$ after which the increase is reduced at $\omega_{T,den}$. The penalty function $W_T(s)$ is selected to have effect at higher frequencies than $W_S(s)$, which is obtained by a proper selection of the frequencies of each transfer function. Finally

$$W_{\bar{u}}(s) = \frac{s + \omega_{\bar{u},num}}{s + \omega_{\bar{u},den}}, \tag{58}$$

is selected, where $\omega_{\bar{u},num}$ and $\omega_{\bar{u},den}$ are very close angular breakpoints that are much larger than the bandwidths of $W_S(s)$ and $W_T(s)$. This ensures that $W_{\bar{u}}(s)$ is proper, very close to 1 and hence does not affect the design. The above selections result in a controller of order 10.

Table 1

Block	Parameter	Numerical value
Search	$grid_{\mathcal{L}_2}$	`logspace(-1.5,0.6,25)`
Search	$grid_q$	`logspace(-2.0,1.0,25)`
Search	$grid_\omega$	`logspace(-2.0,2.0,25)`
H_∞	$grid_\gamma$	`logspace(-0.5,0.5,500)`
$G_p(s)$	ε	0.1 s^{-1}
$F_y(s)$	T_p^d	`logspace(-1.5,0.5,25)`
$F_y(s)$	$W_S(0)$	`logspace(0.0,1.5,25)`
$F_y(s)$	$\omega_{S,num}$	6.0 s^{-1}
$F_y(s)$	$\xi_{S,den}$	1.0
$F_y(s)$	$\omega_{S,den}$	0.5 s^{-1}
$F_y(s)$	$\xi_{T,num}$	1.0
$F_y(s)$	$\omega_{T,num}$	6.0 s^{-1}
$F_y(s)$	$\xi_{T,den}$	1.0
$F_y(s)$	$\omega_{T,den}$	60.0 s^{-1}
$F_y(s)$	$\omega_{\bar{u},num}$	1001.0 s^{-1}
$F_y(s)$	$\omega_{\bar{u},den}$	1000.0 s^{-1}

As a prerequisite for the next step the conditions of the previous analysis are reviewed. A1 holds since the state space representation of (58) must have a nonzero direct term $D_{W_{\bar{u}}}$. A2 is checked in the controller computation since $\mathbf{A}$ and therefore $\tilde{\mathbf{A}}$ varies when (50) is run. A3 is a system assumption. A4 holds by (52), while A5 is checked in the controller computation. As stated above the assumptions A6 and A7 are secured by a sufficiently high frequency roll-off of the frequency functions of the involved signals. A8 is checked in the computation of the stability region. A9 is implied by (52), while A10 is checked after each H_∞ controller computation in the computation of the stability region. Hence it can be concluded that the underlying assumptions of the analysis are valid for the example system. Theorem 1, Theorem 2 and Theorem 3 can therefore be used.

In order to be able to select a suitable controller, the $\mathcal{L}_2$ stability region was computed using the algorithm (50). To do so, the transfer functions of (52), (55), (56), (57) and (58) were first written in the state space form of (15)-(20). The quantities needed for solution of the H_∞ problem of Lemma 1 were then computed as described in section 3.4. Theorem 2 indicates that there are three key parameters that control the $\mathcal{L}_2$ stability region. These are the low frequency gain of the sensitivity function, $W_S(0)$, the designing delay of the plant, T_p^d and the actual delay of the plant, T_p. The set of design variables was therefore selected as

$$\theta_d = (W_S(0) \;\; T_p^d). \tag{59}$$

The actual delay T_p quantifies the stability region as stated in (50).

The H_∞ controller was computed with a numerical search for the minimal γ that solves the Riccati equation of Lemma 1, and that results in a well posed and stable system. See e.g. [7] for details on this well known algorithm. The grids used for computation of the stability region appear in Table 1, together with the parameters of the plant, delay approximation and penalty functions.

Using the above parameters (50) was run. The resulting $\mathcal{L}_2$ stability region is depicted in Fig. 5. The figure supports the theoretical result of Theorem 2 since $\mathcal{L}_2$ stability is not possible for high gains. The approach towards the asymptotic result is also evident from Fig. 5, since the low frequency gain limitation becomes more stringent with increasing designing delay. The allowable delay T_p of the plant, i.e. the robustness, decreases when the designing delay

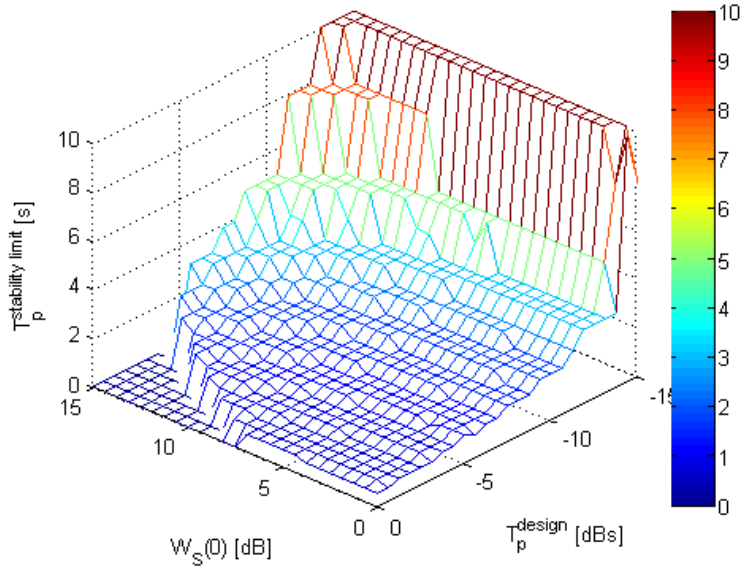

Fig. 5. The $\mathcal{L}_2$ stability region.

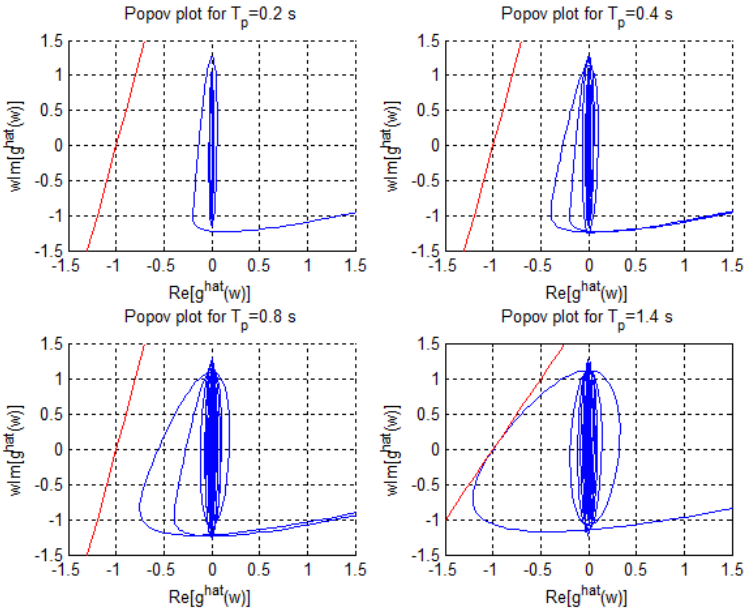

Fig. 6. Popov plots for varying T_p.

T_p^d increases. This is not surprising since delay compensation for performance necessarily becomes very dependent on the assumption of the actual delay. The consequence is that robustness may become worse.

To illustrate the obtained result further, the closed loop system was studied for $W_S(0) = 15dB$ and $T_p^d = 0.200s$, using the parameters of Table 1. As can be seen in Fig. 5, the gain and designing delay are close to the region were the low frequency becomes too large to allow $\mathcal{L}_2$ stability. It is therefore of interest to quantify the stability robustness exactly by means of Popov plots. Such plots appear in Fig. 6, for $T_p = 0.2$ s, $T_p = 0.4$ s, $T_p = 0.8$ s and $T_p = 1.4$ s. It can be concluded that the system is globally $\mathcal{L}_2$ stable for delays in the interval $[0.0, 1.4]$ s. It can also be noted that the low frequency shape of the Popov plot is better adapted to meet the Popov criterion than the corresponding plot of the lead-lag link of [31]. Fig. 5.

The resulting closed loop system dynamics appears in Fig. 7. The bandwidth is about 2 radians/s which indicates a

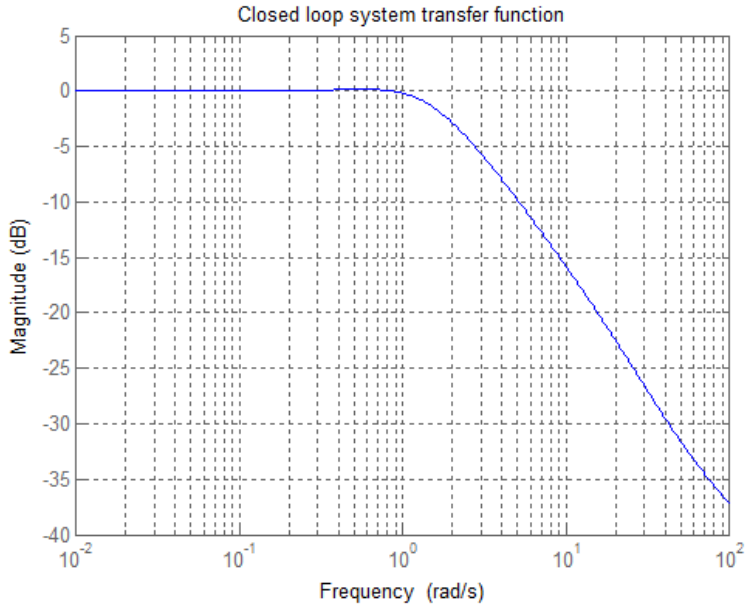

Fig. 7. The closed loop gain of the system, disregarding the saturation.

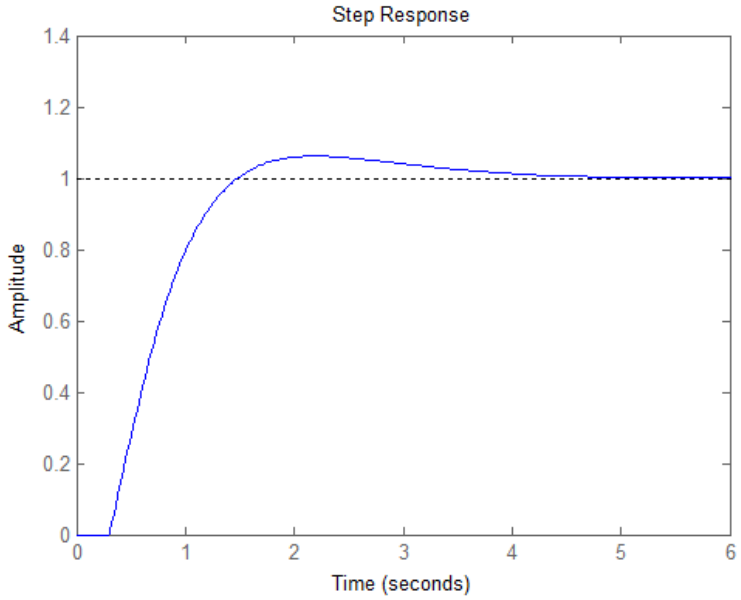

Fig. 8. Step response of the closed loop system.

settling time of a little over 1 s, as shown in Fig. 8. To analyse the low frequency properties and the ability to suppress disturbances, the sensitivity function depicted in Fig. 9 is useful. The sensitivity function follows the low frequency specification, thereby supporting the rule to avoid very low low frequency gains and pure integrating control in the networked situation with long delay and saturation. The robustness specification of $W_T(s)$ is also met, as shown in Fig. 10.

It can be noted that in order to meet the low frequency specification one role of $F_y(s)$ is to attenuate the low frequency gain, a fact that is evident from (52), Table 1 and Fig. 11. The ripple for higher frequencies reduce the effect of resonant poles caused by the delay, c.f. [31]. This provides evidence for the difficulty of this misleadingly

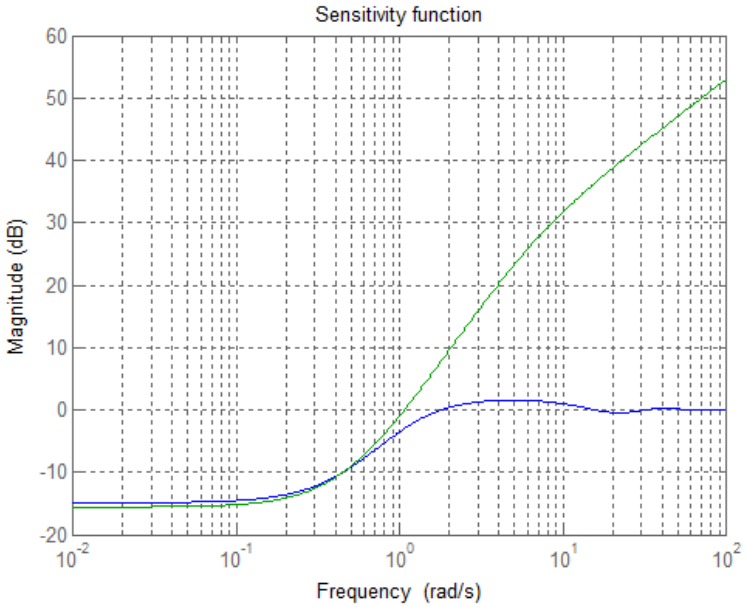

Fig. 9. The sensitivity function of the system (blue), together with the specification $W_S^{-1}(s)$ (green).

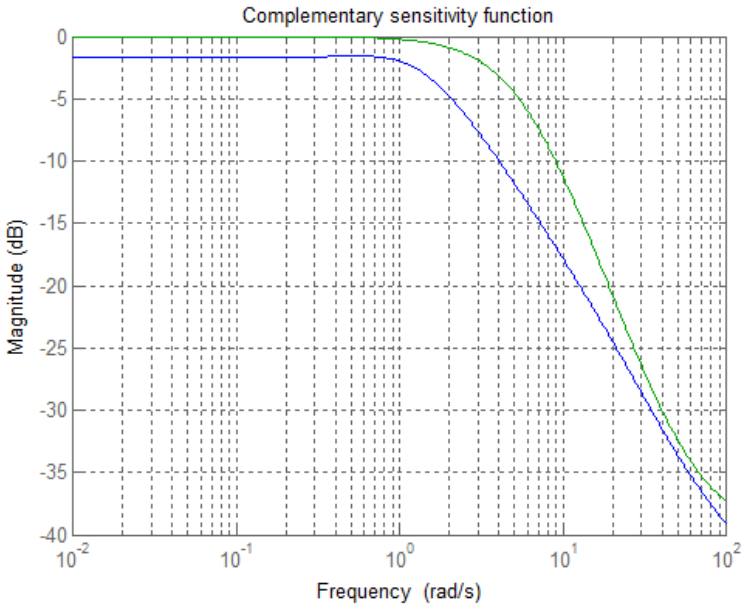

Fig. 10. The complementary sensitivity function of the system (blue), together with the specification $W_T^{-1}(s)$ (green).

simple control problem, the reason being the infinite number of poles of e^{-sT_p}, some of them very resonant [31].

8 Conclusions

The report treated robust networked feedback control. A case with linear plant dynamics, a long and uncertain delay, together with a saturating static nonlinearity was considered. Global closed loop stability was a key design objective, motivated by the fact that in the majority of engineering applications systems need to operate according to specifications at all times.

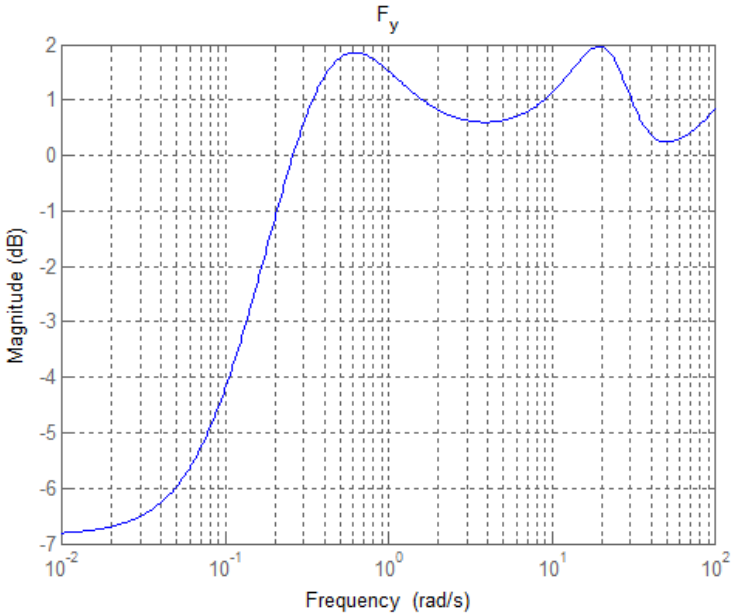

Fig. 11. The transfer function $F_y(s)$ of the controller.

The report first proved that when the delay increases, the Popov criterion can only imply $\mathcal{L}_2$-stability if the low frequency loop gain is bounded. This fact then implies that the low frequency gain of the sensitivity function cannot be arbitrarily small. This theorem is the main result of the report.

Based on the main result a new constraint on the frequency domain penalty on the sensitivity function was formulated. The proposed controller design strategy first selects frequency domain penalties consistent with the new constraint, thereby adapting the employed H_∞ controller design to the case with long delay and saturation. To select a controller, the $\mathcal{L}_2$ stability region is then pre-computed by a new algorithm, by solving the H_∞ control problem over a multidimensional grid of the most interesting design variables and system parameters. Selection of a point in the stability region then gives a globally stable controller with well defined robustness properties.

The proposed controller design performed well when tried on a networked data flow control problem between two internet nodes. The robustness properties appear to be better than for a previously applied lead-lag design. A reason for this could be the additional degrees of freedom of the robust design, since the higher order e.g. allows much better high frequency uncertainty attenuation.

A remaining issue is that the Popov criterion is not necessary for stability. Further research is needed to clarify these aspects. It would also be interesting to apply the methodology to plants with different dynamics. As stated in the introduction, various flow control problems is one possibility. Also servo control problems with delays are interesting since a servo controller is often designed for operation with saturation in order to fully exploit the actuator hardware.

References

[1] K. J. Åström and B. Wittenmark, *Adaptive Control*, Addison-Wesley, Reading, MA, (1989).

[2] J. Baillieul, "Feedback coding for information based control: Operating near the data-rate limit", *in Proc. CDC*, Las Vegas, NV, Dec. 2002, pp. 3229-3236.

[3] A. E. Bryson and Y.-C. Ho, *Applied Optimal Control - Optimization, Estimation and Control*. Hemisphere:NY, New York, 1975.

[4] M. Cea and G. C. Goodwin, "An MPC-based nonlinear quantizer for bit rate constrained networked control problems with application to inner loop power control in WCDMA", *Proc. IEEE CCA*, pp. 153-158, Dec. 19 - 21, Santiago, Chile, 2011.

[5] E. Cheres, Z. J. Palmor and S. Gutman, "Quantitative measures of robustness for systems including delayed perturbations", *IEEE Trans. Automat. Contr.*, vol. 34, no. 11, pp. 1203-1204, 1989.

[6] J. C. Doyle, B. A. Francis and A. R. Tannenbaum, *Feedback Control Theory*. New York, NY: Macmillan, 1992.

[7] T. Glad and L. Ljung, *Reglerteknk, Grundläggande Teori*. Lund, Sweden: Studentlitteratur 1989. (in Swedish)

[8] G. C. Goodwin, H. Haimovich, D. E. Quevedo and J. S. Welsh, "A moving horizon approach to networked control system design", *IEEE Trans. Automat. Contr.*, vol. 49, no. 9, pp. 1427-1445, 2004.

[9] G. C. Goodwin, D. Quevedo and E. I. Silva, "Architectures and coder design for networked control systems", *Automatica* , vol. 44, no. 1, pp. 248-257, 2008.

[10] G. C. Goodwin, M. M. Seron and J. A. DeDona, *Constrained Control and Estimation - An Optimization Approach.* Lomdon, UK:Springer-Verlag, 2005.

[11] G. C. Goodwin and K. S. Sin, *Adaptive Filtering Prediction and Control.* Mineola, NY: Dover, 2009.

[12] G. C. Goodwin, E. I. Silva and D. E. Quevedo, "Analysis and design of networked control systems using the additive noise model methodology", *Asian J. Contr.*, vol. 12, no. 4, pp. 443-459, 2010.

[13] F.-S. Ho and P. Ioannou, "Traffic flow modeling and control using artificial neural networks", *IEEE Control Systems*, vol. 16, no. 5, pp. 16-26, 1996.

[14] M. Jankovic, "Control Lyapunov-Razumikhin functions and robust stabilization of time delay systems", *IEEE Trans. Automat. Contr.*, vol. 46, no. 7, pp. 1048-1060, 2001.

[15] U. Jönsson and A. Rantzer, "Optimization of Integral Quadratic Constraints", *in Advances in Linear Matrix Methods in Control, ed. L. E. Ghaoui and S.-I. Niculescu.* Philadelphia, PA: SIAM, 2001.

[16] B. -K. Lee, H. -W. Chen and B. -S. Chen, "Power control of cellular radio systems via robust Smith prediction filter", *IEEE Trans. Wireless Comm.* vol. 3, pp. 1822-1831, 2004.

[17] G. -P Liu, Y. Xia, D. Rees and W. Hu, "Design and stability criteria of networked predictive control systems with random network delay in the feedback channel", *IEEE Trans. Systems, Man, and Cybernetics, Part C Applications and Reviews*, vol. 37, no. 2, pp. 173-184, 2007.

[18] G. N. Nair and R. J. Evans, "Stabilization with data-rate-limited feedback: tightest attainable bound", *Syst. Contr. Lett.*", vol. 41, no. 1, pp. 49-56, 2000.

[19] D. E. Quevedo and T. Wigren, "Design of embeeded filters for inner-loop power control in wireless CDMA communication systems", *Asian J. Contr.*, vol. 14, no. 4, pp. 891-900, 2012.

[20] V. M. Popov, "Nouveaux criteriums de stabilité pour les systemés automatiques non-linèaries", *Revue d´Electrotechnique et d´Energetique, Acad. de la Rep. Populaire Romaine*, vol. 5, no. 1, 1960.

[21] T. S. Rappaport, "The renaissance of wireless communications in the massively broadband era", Plenary talk, IEEE VTC-2012 Fall, Quebec City, Quebec, Cananda, Sep. 3-6, 2012.

[22] T. S. Rappaport, R. W. Heath Jr., R. C. Daniels and J. N. Murdock, *Millimeter Wave Wireless Communications.* Westford, Massachusetts: Prencice Hall, 2014.

[23] I. W. Sandberg, "A frequency-domain condition for the stability of feedback systems containing a single time-varying element", *Bell Sys. Tech. J.*, vol. 43, pp. 1601-1608, 1964.

[24] E. I. Silva, D. Quevedo and G. C. Goodwin, "Optimal controller design for networked control systems", *Proc. 17:th IFAC World Congress*, COEX, South Korea, pp. 5167-5172, 2008.

[25] R. Srikant and L. Ying, *Communication Networks - An Optimization, Control and Stochastic Networks Perspective*. Padstow Cornwall, UK: Cambridge Univeristy Press, 2014.

[26] M. Sternad, "Optimal and adaptive feedforward regulators", Ph.D dissertation, *Department of Technology, Uppsala Univ.*, Uppsala, Sweden, May, 1987.

[27] M. Sternad and T. Söderström, "LQG-optimal feedforward regulators", *Automatica*, vol. 24, pp. 557-561, 1988.

[28] M. Vajta, "Some remarks on Padé approxoimations", *in Proc. third TEMPUS-INTCOM Symposium*, Veszprém, Hungary, Sep. 9-14, 2000.

[29] N. Vandelli, D. Wroblewski, M. Velonis, T. Bifano, "Development of a MEMS microvalve array for fluid flow control", *J. of Microelectromechanical Systems*, vol. 7, no. 4, pp. 395-403, 1998.

[30] M. Vidyasagar, *Nonlinear Systems Analysis.* Englewood Cliffs, NJ: Prentice-Hall, 1978.

[31] T. Wigren, "Robust $\mathcal{L}_2$-stable networked control of wireless packet queues over delayed internet connections",*IEEE Trans. Contr. Sys. Tech., submitted*, November, 2014.

[32] G. Zames, "On the input-output stability of time-varying nonlinear feedback systems, Part1: Conditions derived using concepts of loop-gain, conicity and positivity", *IEEE Trans. Automat. Contr.*, vol. AC-11, pp. 228-238, 1966.

[33] K. Zhou, J. C. Doyle and K. Glover, *Robust and Optimal Control.* Upper Saddle River, NJ: Prenctice Hall, 1996.

A Proof of theorem 1

It is first noted that Fig. 2 is equivalent to Fig. 3, by (33)-(35). It is hence sufficient to study the block diagram of Fig. 3. Since Lemma 2 is valid for the block diagram of Fig. 4, the first step of the proof is to transform Fig. 3 to the structure of the block diagram of Fig. 4.

To achieve this, the delay appearing after the static nonlinearity is moved to appear before the nonlinearity. This is allowed since the nonlinearity is time invariant. After the transformation the delay operator is moved into the two

branches of the summation point. This is represented by a multiplication of $F_y(s)$ and $L_{\infty,r}$ with e^{-sT_p}. With these changes, the signal $u(s)$ of Fig. 3 is considered. Since this signal is the same as the signal $e_2(s)$ of Fig. 4, it follows that

$$e_2(s) = u(s) = e^{-sT_p} L_{\infty,r} y_{ref}(s)$$

$$-e^{-sT_p} F_y(s) w(s) - e^{-sT_p} F_y(s) G_p(s) y_2(s), \tag{A.1}$$

where the signal $y_2(s)$ appears at the output of the static nonlinearity as defined by Fig. 4. Rearranging (A.1) then gives

$$e_2(s) = e^{-sT_p} L_{\infty,r} y_{ref}(s)$$

$$+e^{-sT_p} F_y(s) G_p(s) \left(-\frac{1}{G_p(s)} w(s) - y_2(s) \right). \tag{A.2}$$

A similar calculation based on Fig. 4 gives

$$e_2(s) = u_2(s) + \hat{g}(s)(u_1(s) - y_2(s)). \tag{A.3}$$

A comparison of (A.2) and (A.3) then gives

$$u_1(s) = -\frac{1}{G_p(s)} w(s), \tag{A.4}$$

$$u_2(s) = e^{-sT_p} L_{\infty,r} y_{ref}(s) \tag{A.5}$$

$$\hat{g}(s) = e^{-sT_p} F_y(s) G_p(s). \tag{A.6}$$

It remains to prove that the technical conditions of Lemma 2 hold. Because of A3, A4 and A5 all poles of the time invariant transfer function $\hat{g}(s)$ of (A.6) are in the interior of the left half plane. Since $F_y(s)$ is strictly proper and since A4 holds it follows that $\hat{g}(s)$ is strictly proper and hence $s\hat{g}(s)$ is at least proper. It then follows that $g(\cdot) \in \mathcal{A}$ and $\dot{g}(\cdot) \in \mathcal{A}$, see Definition 4.

By A4 and A7 the right hand side of (A.4) is proper and asymptotically stable and is therefore in $\mathcal{L}_2$. It follows that $u_1 \in \mathcal{L}_2$. This is a necessary conclusion here since it is a prerequisite for stating $\mathcal{L}_2$ stability in Lemma 2, cf. Definition 3.

By A6 $y_{ref} \in \mathcal{L}_2$ and $\dot{y}_{ref} \in \mathcal{L}_2$. The same is therefore true for the right hand side of (A.5). It follows that $u_2 \in \mathcal{L}_2$ and $\dot{u}_2 \in \mathcal{L}_2$.

Observing that the static nonlinearity $\Phi(.)$ obeys (38) completes the proof.

B Proof of theorem 2

Since A4, A5, A9 and A10 hold, $|\hat{g}_o(j\omega)| \neq 0$, and it follows from (43) and (44) that

$$\arg(\hat{g}_o(j\omega_l)) - \omega_l T_p = \pm l\pi, \quad l = 1, ..., n_0, ..., \tag{B.1}$$

where l is odd and n_0 is an odd number that is guaranteed to exist due to A8. Note that the evaluation of transfer function values on the negative real axis are hence tied to ω_l.

The conditions A4, A5, A9 and A10, together with (45) and (46) imply that $\arg(\hat{g}_0(j\omega)) < \varphi_0 < \infty$. Furthermore, by A4 and since $F_y(s)$ is strictly proper by construction, it follows that $|\hat{g}_o(j\omega)| \to 0$ as $\omega \to \infty$. Therefore there is a

largest n_0 of (B.1) and a maximal $\omega_m(n_0)$, for which $Re[\hat{g}(j\omega_m(n_0))] \leq -1/k$, i.e for which the Popov criterion does not hold. The fact that n_o is finite implies that

$$\omega_l = \frac{1}{T_p}\left(\arg(\hat{g}_o(j\omega_l)) \pm l\pi\right), \quad l = 1, ...n_0. \tag{B.2}$$

Equation (B.2) applied to $\omega_m(n_0)$ then gives

$$\lim_{T_p\to\infty} \omega_m(n_0) = \lim_{T_p\to\infty} \omega_{n_0}$$

$$= \lim_{T_p\to\infty} \frac{1}{T_p}\left(\varphi_0 \pm n_0\pi\right) = 0. \tag{B.3}$$

To proceed the following Lemma is useful

Lemma B: Assume that

$$h(s) = K\frac{(s+z_1)...(s+z_m)}{(s+p_1)...(s+p_n)},$$

where complex zeros and poles appear as complex conjugate pairs. Then

$$\lim_{\omega\to 0} Re[h(j\omega)] = K\frac{z_1...z_m}{p_1...p_n}$$
$$\lim_{\omega\to 0} Im[h(j\omega)] = 0.$$

Proof: A straightforward computation gives

$$Re[h(j\omega)] = K\frac{z_1...z_m\bar{p_1}...\bar{p_n} + \omega^2(...}{(\omega^2+|p_1|^2)...(\omega^2+|p_n|^2)} \tag{B.4}$$

$$Im[h(j\omega)] = K\frac{\omega(...}{(\omega^2+|p_1|^2)...(\omega^2+|p_n|^2)}, \tag{B.5}$$

where $\bar{p_i}$ denotes the complex conjugate of p_i. Letting $\omega \to 0$ gives the result of Lemma B.

Next, using the conclusion (B.3) and applying Lemma B to $\hat{g}_o(j\omega_l)$ where $\omega_l \leq \omega_m(n_0)$, results in

$$\lim_{T_p\to\infty} \arg(\hat{g}_o(j\omega_l)) = 0, \quad l = 1, ..., n_0. \tag{B.6}$$

Therefore it follows from (B.1) and (B.2) that

$$\lim_{T_p\to\infty} \omega_l T_p = \pm l\pi, \quad l = 1, ..., n_0. \tag{B.7}$$

Exploiting (42) and Lemma B implies that

$$\lim_{T_p\to\infty} Re[\hat{g}(j\omega_l)] = \lim_{T_p\to\infty} Re[e^{-j\omega_l T_p}\hat{g}_o(j\omega_l)]$$

$$= \lim_{T_p\to\infty} \left(\cos(\omega_l T_p)Re[\hat{g}_o(j\omega_l)] - \sin(\omega_l T_p)Im[\hat{g}_o(j\omega_l)]\right)$$

$$= -\lim_{T_p\to\infty} Re[\hat{g}_o(j\omega_l)], \quad l = 1, ...n_0. \tag{B.8}$$

By (B.2) and (B.3) the last equation can be written

$$\lim_{T_p \to \infty} Re[\hat{g}(j\omega_l)]$$

$$= - \lim_{\omega_l \to 0} Re[\hat{g}_o(j\omega_l)], \quad l = 1, ..., n_0. \tag{B.9}$$

By Theorem 1, the Popov criterion hence cannot hold in the high delay limit if

$$\lim_{T_p \to \infty} Re[\hat{g}(j\omega_l)]$$

$$= - \lim_{\omega_l \to 0} Re[\hat{g}_o(j\omega_l)] \leq -1/k, \quad l = 1, ..., n_0, \tag{B.10}$$

i.e if

$$\lim_{\omega_l \to 0} Re[\hat{g}_o(j\omega_l)] > 1/k, \quad l = 1, ..., n_0. \tag{B.11}$$

By Theorem 1, (45), (46) and Lemma B, the limiting value of (B.11) can be expressed as

$$\lim_{\omega_l \to 0} Re[\hat{g}_o(j\omega_l)] \tag{B.12}$$

$$= G_{p,o} F_{y,o} \frac{b_1 ... b_{nb} d_1 ... d_{nd}}{a_1 ... a_{na} c_1 ... c_{nc}}, \quad l = 1, ..., n_0. \tag{B.13}$$

This completes the proof of Theorem 2.